JGR Space Physics

RESEARCH ARTICLE
10.1029/2020JA028622

Multi-Wavelength Imaging Observations of STEVE at Athabasca, Canada

Sneha Yadav[1], Kazuo Shiokawa[1], Yuichi Otsuka[1], Martin Connors[2,3,4], and J.-P. St Maurice[3,5]

[1]Institute for Space-Earth Environmental Research, Nagoya University, Nagoya, Japan, [2]Athabasca University Observatories, Athabasca University, Athabasca, Alberta, Canada, [3]Department of Physics and Astronomy, University of Western Ontario, London, ON, Canada, [4]Department of Physics and Astronomy, University of Calgary, Calgary, AB, Canada, [5]Department of Physics and Engineering Physics, University of Saskatchewan, Saskatoon, Saskatchewan, Canada

Key Points:

- First study of multi-wavelength imaging observations of strong thermal emission velocity enhancement (STEVE) where the arc detached from the auroral oval both in red and green lines
- STEVE arc is found to be embedded in a region of diffuse red and green emission
- STEVE arc detachment, its equatorward movement and brightness coincided with the sudden change in magnetic activity

Supporting Information:

- Supporting Information S1
- Figure S1
- Figure S2
- Movie S1
- Movie S2
- Movie S3
- Movie S4
- Movie S5
- Movie S6

Correspondence to:
S. Yadav,
sneha.yadav84@gmail.com

Citation:
Yadav, S., Shiokawa, K., Otsuka, Y., Connors, M., & St Maurice, J.-P. (2021). Multi-wavelength imaging observations of STEVE at Athabasca, Canada. *Journal of Geophysical Research: Space Physics*, *126*, e2020JA028622. https://doi.org/10.1029/2020JA028622

Received 24 AUG 2020
Accepted 12 NOV 2020

Abstract We present the first multi-wavelength imaging observations of strong thermal emission velocity enhancement (STEVE) using an all-sky imager at Athabasca (magnetic latitude = 61.5°N), Canada. This study is based on three STEVE events which were accompanied by picket fence structures in the green-line. Although the STEVE arc was dominant in 630 and 557.7-nm, weak emissions were also found in other wavelengths including OI at 844.6, Hβ, Na, and the nominal background filter at 572.5-nm. As observed at 630 and 557.7-nm, the STEVE arc started as a faint arc close to the auroral oval and moved equatorward. The 557.7-nm arc exhibited picket fence structure at later times after it moved equatorward. The picket fence was sometimes found to persist even after the 630-nm arc had disappeared. During a particular event, the STEVE arcs in both the 630 and 557.7-nm were found to carry a ribbon-like motion moving along the arc. We have found that STEVE arcs are embedded in a region of weak diffuse auroral emissions. The STEVE arcs have sharp boundaries and these boundaries are different in red- and green-line. The sharp decrease in the intensity at the immediate poleward edge of the STEVE arc appears as a "dark-band" in the green-line images. Based on the horizontal component of the geomagnetic field at Fort Smith (magnetic latitude 67.28°N), we find that the STEVE arc detachment, its equatorward motion, and its brightness coincided with changes in the magnetic activity during the recovery phase of a substorm.

1. Introduction

Strong thermal emission velocity enhancements (STEVEs) is a relatively new phenomenon in the area of auroral physics. Although STEVE has been recognized by amateur night sky watchers for about a decade, it is only recently that it has drawn attention of the space physics community. STEVE is distinctly different from traditional aurora and appears as a violet and green narrow luminous band extending over thousands of kilometers in the east-west direction. The first scientific report that shed light on the background ionospheric conditions during STEVE was published by MacDonald et al. (2018). Based on one event, they reported that STEVE structures were associated with an unusual rise in electron temperature and a deep F region density depletion, along with a strong westward ion flow, suggesting that STEVE is an optical manifestation of subauroral ion drift (SAID). This study was supported by the findings of Archer, Gallardo-Lacourt, et al. (2019) which presented eight STEVE events associated with SAID.

In optical data, STEVE is likewise identified as a latitudinally narrow band of luminosity but extended in longitude (thousands of kilometers in east-west direction) and located in the subauroral region (Gallardo-Lacourt, Liang et al., 2018; Gallardo-Lacourt, Nishimura, et al., 2018). By using time history of events and macroscale interactions during substorms (THEMIS) all-sky imager and the redline emission geospace observatory (REGO) database, Gallardo-Lacourt, Nishimura, et al. (2018) reported that the STEVE arc detaches from the auroral oval and moves equatorward. MacDonald et al. (2018) first pointed out that purple luminosity in STEVE might represent a mixture of exotic emissions that are not included in the wavelengths known to dominate in the precipitating electron auroral luminosity. Later, Gillies et al. (2019) studied the spectral characteristics of STEVE and the picket fence structures by using the transition region explorer (TREx) Spectrograph at Lucky Lake, Saskatchewan. Their study provided evidence of the continuum nature of STEVE and reported an overall enhancement of a continuous spectrum spanning between ~400 and

730 nm along with an enhancement of the OI red-line (630-nm) during STEVE. "Picket Fences" are distinct structures seen in the green-line of oxygen which may accompanies the purple STEVE emission. These green structures occur at altitudes lower than STEVE (Archer, St.-Maurice, et al., 2019; Liang et al., 2019) and physical processes responsible for the occurrence of these structures were suggested to be precipitating electrons, different from those suggested for the 630-nm emission (Nishimura et al., 2019). A recent study by Liang et al. (2019) revealed that STEVE is emitted from two distinctly different altitude regions with a higher elevation STEVE from ∼250 km and a lower elevation STEVE from ≤150 km altitude. Archer, St.-Maurice, et al. (2019) showed that the altitude spread of STEVE was between 130 and 270 km and that picket fences extend between 95 and 150 km. Earlier studies merely showed the presence of green picket fence structure in a fully developed stage and did not focus on the characteristics of its evolution.

Nishimura et al. (2019) presented three STEVE events by analyzing THEMIS all-sky images and investigated the role of particle precipitation during STEVE using defense meteorological satellite program (DMSP) and Swarm satellites. They reported that the STEVE event with the picket fence was associated with substantial electron precipitation at energies of >∼1 keV. However, such precipitation was found to be absent for events without picket fence and instead it manifested as with a localized enhancement of <100 eV electrons. Mende et al. (2019) refuted the precipitation hypothesis of Nishimura et al. (2019) and suggested that picket fences are manifestations of suprathermal electrons. The study of Gallardo-Lacourt, Liang, et al. (2018) using Polar Orbiting Environmental Satellite showed the complete absence of particle precipitation (electrons or ions) for a STEVE event. These studies asserted that the STEVE arc is a result of ionospheric processes driven by strong electron heating in the upper F-region ionosphere. Chu et al. (2019) revealed a new aspect of STEVE by showing that STEVE is not only located at the sharp plasmapause boundary where quasi-static SAID electric fields are found, but that there is likely an important acceleration of the electrons along the magnetic field lines in response to kinetic Alfvén waves.

The geomagnetic conditions favorable for the formation of STEVE were reported by Gallardo-Lacourt, Nishimura, et al. (2018) using 28 events observed by THEMIS all-sky imager and REGO. They reported that STEVE occurred during the substorm recovery phase, a condition which is similar to formation of Stable Auroral Red (SAR) arcs (Takagi et al., 2018). It is worth mentioning that STEVE arcs are different from SAR arcs because of their unique spectral characteristics. While SAR arcs are dominated by red-line (630-nm) emission with no or very little green-line (557.7-nm) or any other emission, STEVE exhibits a characteristic purple color, sometimes with picket fence structure in the green-line emission lower down.

In this study, we present the first imaging observations of STEVE at multiple wavelengths by using an all-sky cooled charge coupled device (CCD) airglow imager operating at Athabasca, Canada. By using this monochromatic camera with narrow bandpass filters, we present three STEVE events observed in 2019. New insights about STEVE have emerged from our study, based on the new instruments we have brought to the table. These new insights are based on the following unique characteristics of our instruments, namely:

1. As already mentioned above, scientific instruments used to study ground-based optical emissions from STEVE have focused on THEMIS white light cameras, REGO red oxygen line cameras, and TREX spectrometer observations over the range 400–800 nm. By contrast, we have used long term exposures for monochromatic emissions from STEVE in the red and green lines of oxygen and have complemented this with emissions from the background continuum to confirm that the emissions came from STEVE. This has enabled us to study the dynamical properties of the red and green STEVE (i.e., the upper vs. lower STEVE emissions) and of picket fence emissions with a 2 min resolution, including the detection of passing ribbon-like structures moving through STEVE arcs at times.
2. Now that it has become clear that oxygen green-line from STEVE and related picket-fence emissions are from below 150 km altitude, while oxygen red-line emissions from STEVE are strongest around 250 km altitude, the continuous monitoring of these two lines, coupled with a monitoring of the background STEVE continuum through a nonauroral emission allows us to unravel the subtle evolution in the vertical structure of STEVE, as well as its relation to the appearance and disappearance of picket fences.
3. Our continuous monitoring of the oxygen lines of interest over a wide field of view allows us to study the connection between STEVE and the evolving aurora. This includes the connection with the diffuse aurora, which, we will show, overlaps with the region of STEVE emissions.

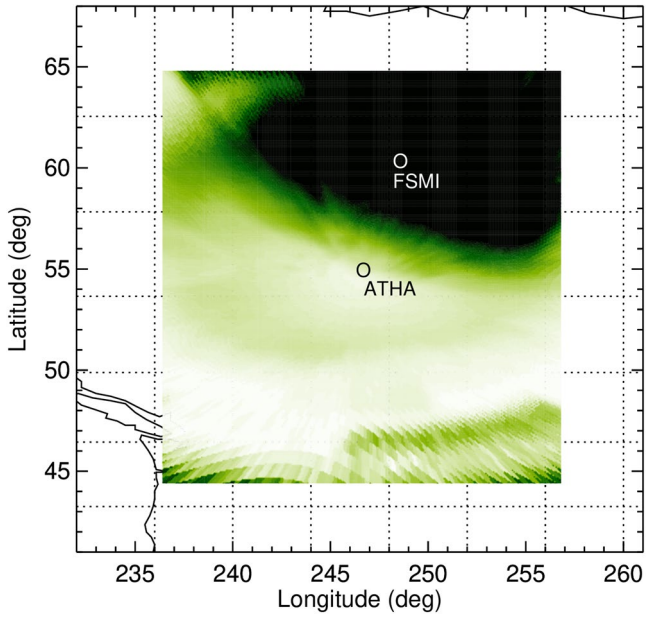

Figure 1. Location of Fort Smith and ASI at Athabasca. The green-line image taken on May 02, 2019 at 0450 UT is superimposed on the map. This image is representative to show the location of two stations with respect to the auroral oval for all three considered events. FSMI is located inside the auroral oval at the longitude zone of Athabasca. ASI, all-sky imager; ATHA, Athabasca; FSMI, Fort Smith.

4. In addition to revealing that STEVE occurs during the substorm recovery phase, Gallardo-Lacourt, Nishimura, et al. (2018) also reported the presence of several auroral streamers at higher latitudes during STEVE. However, the variation of STEVE emissions with respect to changes in the magnetic activity at auroral latitudes is not known. We were able, however, to uncover a connection between the evolution of STEVE and the northward component of the magnetic field perturbation recorded by magnetograms at Fort Smith, Canada, north of Athabasca in the auroral oval.

2. Data and Methodology

The present study relies on the airglow/auroral images obtained by the all-sky imager (ASI) (camera no. 7) operating at Athabasca (54.6°N, 246.3°E, magnetic latitude: 61.5°N, $L = 4.4$), Canada since September 3, 2005. Magnetic midnight for this ASI occurs at ~8.1 UT. It is a part of the Optical Mesosphere Thermosphere Imagers (OMTIs) (Shiokawa et al., 1999, 2009) and has a 180° field-of-view fish-eye lens, six band-pass optical filters, and a thermoelectrically cooled CCD with 512 × 512 pixels. In order to increase the signal-to-noise ratio, CCD images are processed with 2 × 2 binning, so that our images had a resolution of 256 × 256 pixels. This camera has six band-pass filters that allow measurement of airglow/auroral emissions at specific wavelengths: OI at 557.7 nm, OI at 630.0 nm, Hβ at 486.1 nm, Na at 589.3 nm, OH bands at 720–910 nm, OI at 844.6 nm, and nominal background at 572.5 nm. In this study, we have used the images for all the filters including the "nominal background," except for the OH band.

The images at 557.7 nm, 630 nm, 486.1 nm, and Na at 589.3 nm are obtained at a time resolution of 2 min with exposure times of 5 s, 30 s, 40 s, and 15 s, respectively, whereas images at 844.6 nm (exposure time of 25 s) and 572.5 nm (exposure time of 15 s) are acquired at every 15 min interval. In spite of the fact that the all-sky images contain background continuum emission throughout the transmission width of the band-pass filter, we have not removed the background emission from the images. This is because STEVE arc was also observed in background emission images at 572.5 nm and the subtraction of airglow images from the background images might affect the absolute intensity of STEVE. The raw images are projected into the geographical latitude/longitude coordinates by assuming that the emission intensity has a peak at 250 km altitude for 630-nm and 120 km for the other wavelengths (Archer, St.-Maurice, et al., 2019; Liang et al., 2019). We have constructed North-South (NS) keograms by stripping the slices of airglow images at the longitude of Athabasca (246.3°E). The keograms facilitate the study of temporal variations in the auroral emission intensities and their latitudinal motion.

Time shifted 1-min data of interplanetary magnetic field (IMF) By and Bz observed by the WIND satellite were obtained from CDAWeb. Because solar wind measurements are made at the Lagrangian (L1) point by the spacecraft (~220 RE from the Earth), they are shifted to the nose of the bow shock (~14 RE from the Earth) to study the magnetosphere-ionosphere coupling. The details about time-shifting are given on the CDAWeb site. The definitive auroral electrojet (AE) index, which is commonly used to assess the substorm activity, was unavailable for these recent events. However, the quick-look plots showing the variation of AE/AL index are available at the website of WDC, Kyoto. The magnetometer data at Fort Smith (FSMI; Lat 60.0°N, Long 248.2°E; magnetic latitude: 67.28°N) (Mann et al., 2008) were used to examine the variation of its X-component (northward component) in the presence of STEVE. Magnetic midnight at FSMI occurs at ~0800 UT. Figure 1 shows the location of Fort Smith and ASI at Athabasca. The ASI green-line image taken on May 02, 2019 at 0450 UT is superimposed on the map. This image is representative to show the location of two stations with respect to the auroral oval for all three considered events. At the times of interest, Fort Smith was located in the auroral oval poleward of Athabasca. The X-component magnetogram at FSMI represents the substorm activity in the longitude zone of the Athabasca ASI.

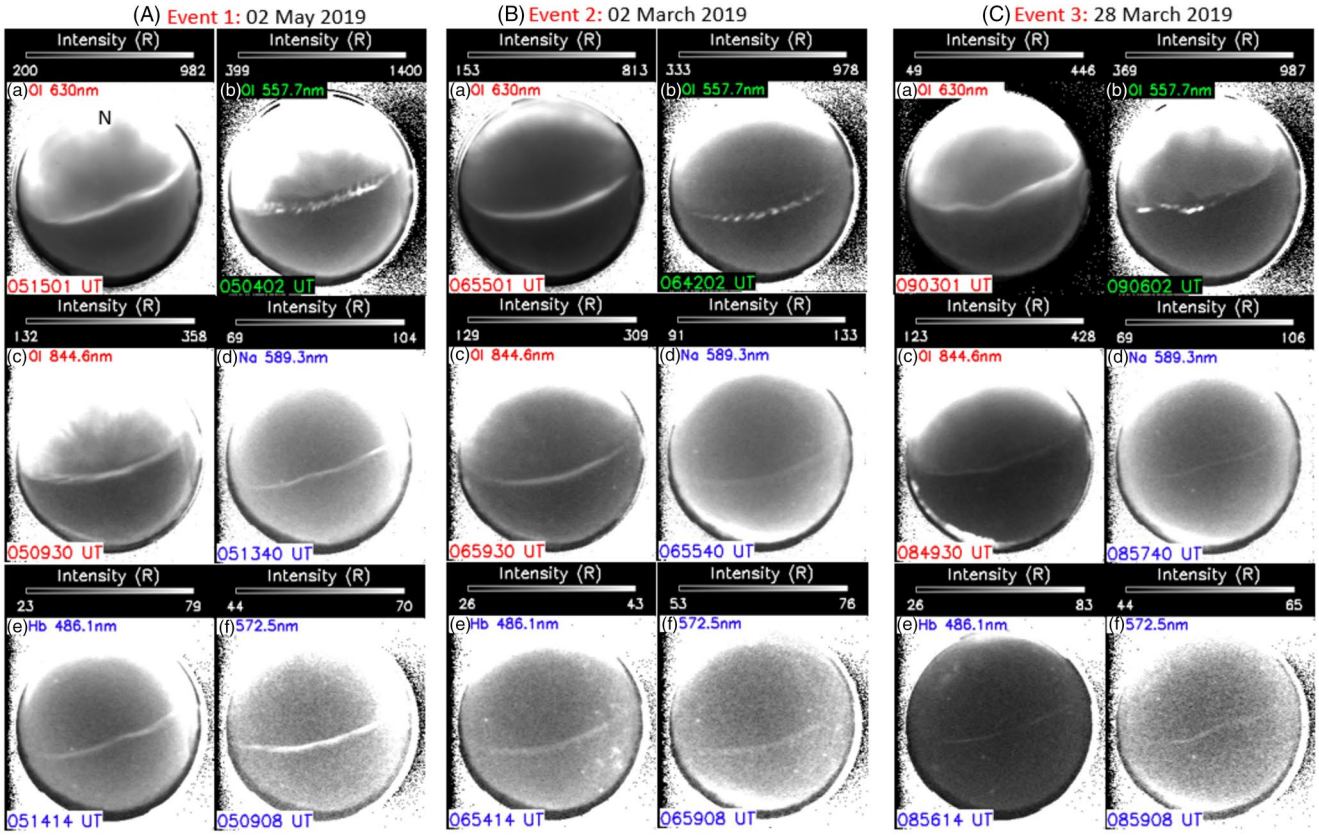

Figure 2. Multiple wavelength observation of STEVE (strong thermal emission velocity enhancement) for three events: (A) May 02, 2019, (B) March 02, 2019, and (C) March 28, 2019. STEVE, strong thermal emission velocity enhancement.

3. Observations

We present three STEVE events observed in the airglow images at multiple wavelengths at Athabasca. To qualify as STEVE, an arc must satisfy three criteria: (1) it must be narrow, (2) equatorward of the main auroral oval, (3) must contain broadband emissions. It should be noted here that at the time of first detection, an arc sometimes does not satisfy all the criteria because it might not be bright enough to be diagnosed as a STEVE proper. However, if the arc evolves into a STEVE then it may well be initially a STEVE. All three events were associated at some point in time with picket fence structures in the green-line emission. The latitudinally narrow STEVE arcs were seen at four other wavelengths (486.1, 572.5, 589.3, and 844.6 nm), asserting the presence of STEVE. The arc in the green-line developed picket fence structures at the later times. Therefore, we have referred the arcs in the red- and green-line as the red and green STEVE arcs, respectively. Figure 2 shows the auroral/airglow images obtained at 630, 486.1, 589.3, 844.6, 572.5, and the 557.7 nm at Athabasca for May 02, 2019 (event 1), March 02, 2019 (event 2), and March 28, 2019 (event 3). Consistent with the earlier studies (e.g., Chu et al., 2019; Gallardo-Lacourt, Liang et al., 2018; Gallardo-Lacourt, Nishimura, et al., 2018; Liang et al., 2019), in all the optical images, STEVE was observed as a structure which is narrow in latitude but extended in longitude, separated from the auroral oval. The images at 557.7-nm show the presence of picket fence structures. STEVE arcs are observed as faint structures in the 589.3, 486.1, 572.5, and 844.6 nm emission lines.

The quick-look plots of AE/AL (not shown here) for all three events show that AE/AL index showed decreasing/increasing trend during the presence of STEVE arc, indicating the presence of a substorm recovery phase. Thus, consistent with the earlier work of Gallardo-Lacourt, Nishimura, et al. (2018), all three STEVE events occurred during the recovery phase of the substorm.

In order to show the background geomagnetic conditions under which STEVE occurred, we present the variation of IMF By and Bz, and the X-component of the magnetic field at FSMI for our three STEVE events in

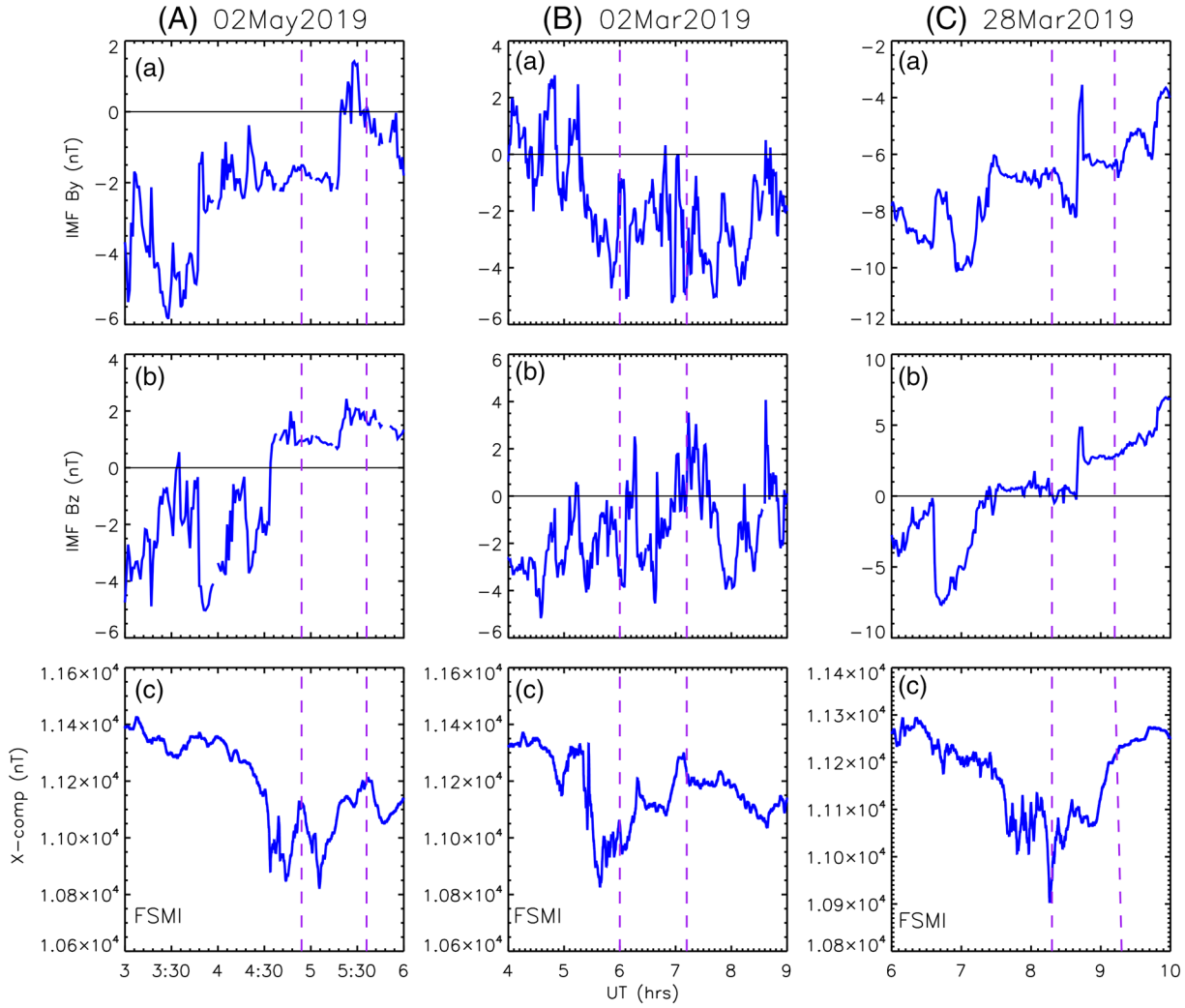

Figure 3. Variation of IMF By (top panel), IMF Bz (middle panel), and X-component (bottom panel) at Fort Smith (FSMI) during three STEVE events: (A) May 02. 2019, (B) March 02, 2019, and (C) March 28, 2019. The interval between the purple dashed lines indicates the duration of arc in the all-sky imager. STEVE, strong thermal emission velocity enhancement.

Figure 3. The interval between the dashed lines in Figure 3 indicates the duration of event that was observed in the optical data. An event is considered to start from the time of appearance of arc in the red-line close to the auroral oval, and its subsequent disappearance in all the lines marks the end of an event. For the events of May 02, 2019 (A) and March 28, 2019 (C), the IMF Bz remained northward throughout the time when STEVE appeared. By contrast, for the STEVE event of March 02, 2019 (B), the IMF Bz remained dominantly southward. The IMF By had generally negative values during all three STEVE events. The X-component at FSMI shows the presence of bay structures in the presence of STEVE, indicating substorm activity. There generally seems to be additional activities in the recovery phase of the substorm during the presence of STEVE. These are observed as abrupt increases or decreases in the X-component at FSMI during the recovery phase of the prevailing substorm.

3.1. Evolution of STEVE Arc and Picket Fence Structure

The temporal evolution of STEVE arcs has been studied by analyzing time sequential images of red (630-nm) and green (557.7-nm) emission lines. The images have been selected at random intervals to represent the temporal evolution of STEVE. The detailed red-line variation of the STEVE arc and of the green-line picket fence can be seen in Movies S1–S6 provided in supplementary material. We have also plotted the NS

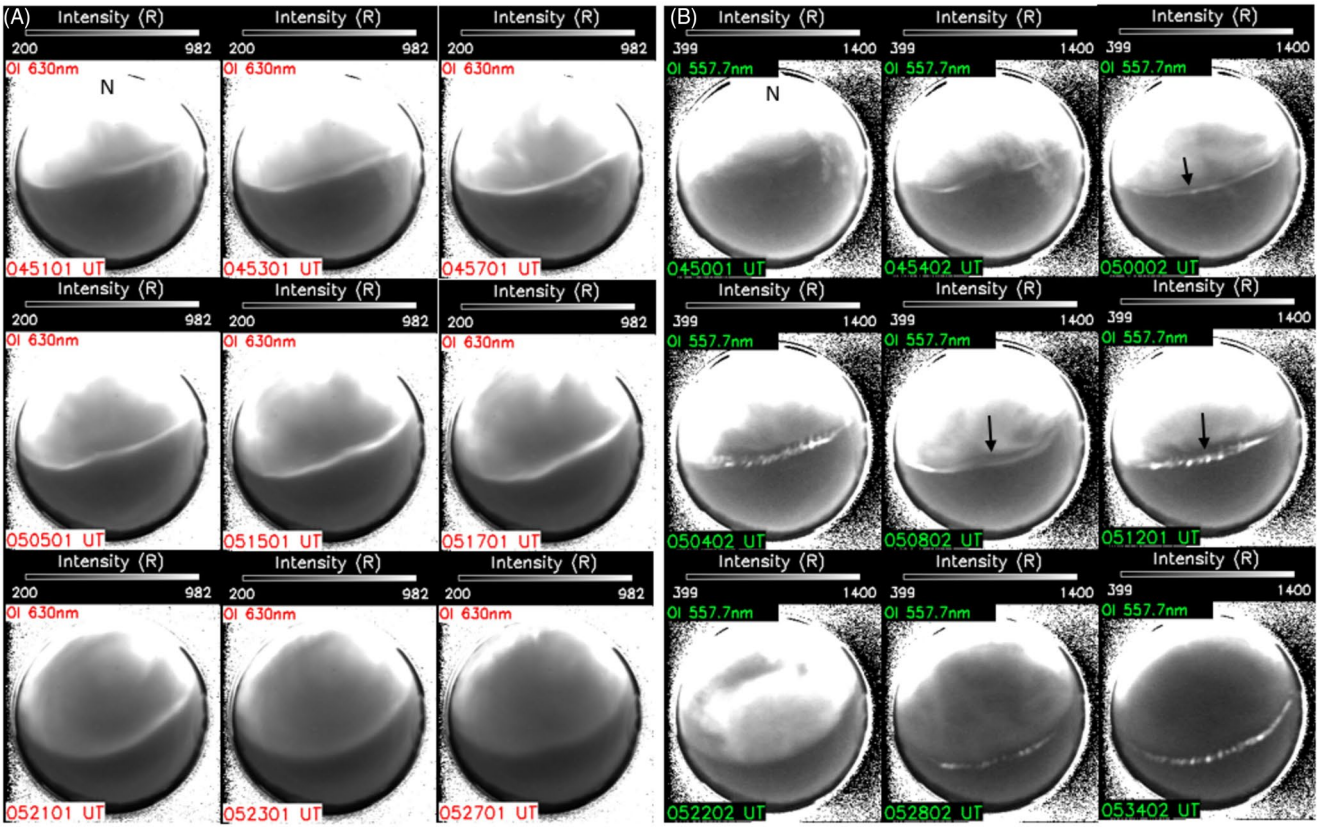

Figure 4. Time sequential images (during ~0450-0530UT) depicting the evolution of STEVE arc in (A) red line (630-nm) and (B) picket fence structure in green line (557.7-nm) for May 02, 2019. Black arrows in the green line images highlight the dark-band at the poleward edge of the arc-structure. STEVE, strong thermal emission velocity enhancement.

keograms for all the emission lines to study the detailed variation of STEVE emissions at different wavelengths. The following subsections describe the evolution of STEVE and picket fence structures for the three events:

3.1.1. Event 1: May 02, 2019

Figure 4a and 4b depict the sequential images in the red and green lines for May 02, 2019. The bright emission in the northern sky of the images for both wavelengths shows the presence of the auroral oval. The images for this case were available from ~0450 UT. At the start of the observations (i.e., from ~0450 UT), a faint arc-like structure (brightening equatorward of the auroral oval) appeared very close to the auroral oval in all considered emission lines including red- and green-line (Figure 4). As time progressed, this faint arc separated itself from the auroral oval and moved equatorward. We have referred this process as "detachment of the arc from the oval." The presence of emission in the nonoxygen lines (Hβ, Na, and background) provides the evidence for STEVE from the beginning of observations. We found that the detachment of a STEVE arc in the green line is similar to the detachment in the red-line, which is something that could not be reported in previous studies. This arc-like structure exhibited a narrow latitudinal width in all the monochromatic images at different wavelengths. After detaching itself from the oval, it shifted equatorward and brightened. The equatorward motion of STEVE is consistent with earlier studies (e.g., Gallardo-Lacourt, Liang, 2018; Gallardo-Lacourt, Nishimura, et al., 2018; Liang et al., 2019). The evolution of the arc in both the red and green lines can clearly be seen in Movies S1 and S2. While the arcs in both the red and green lines exhibit equatorward motion, they also display occasionally wave-like motion along the arc (~0505–0517 UT) during the end phase of their evolution, that is, after the detachment of the arc. Since this quivering motion of STEVE arc is similar to that of a ribbon wavering in the wind, we have referred such motion as "ribbon-like motion". Systematic propagation of the ribbon-like structure cannot be clearly

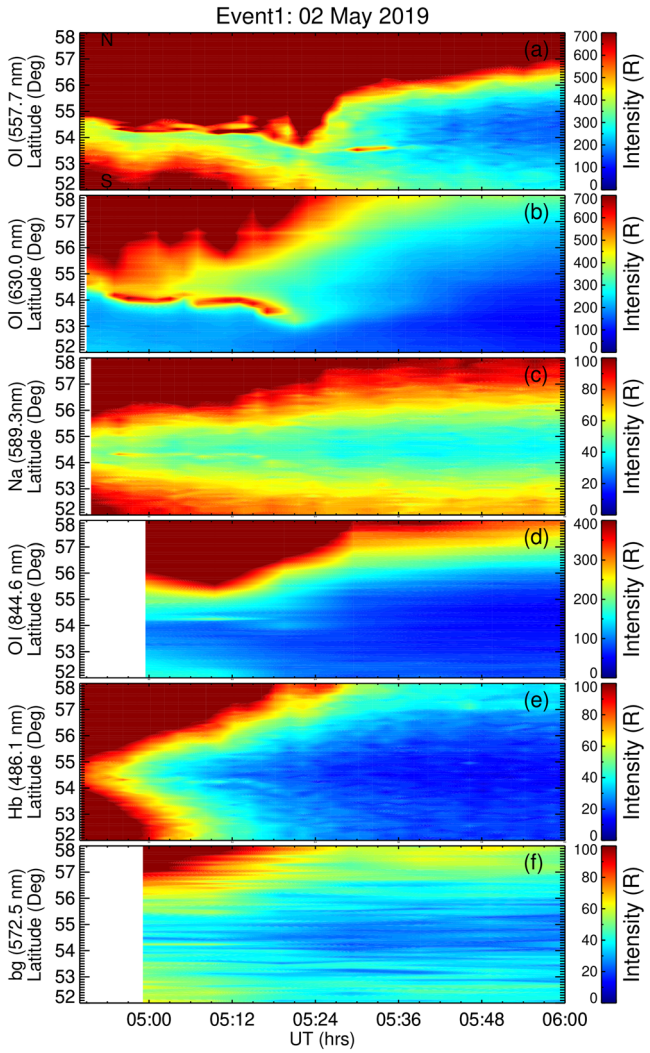

Figure 5. Keograms (in geographic coordinates) depicting the temporal evolution of STEVE at multiple wavelengths for May 02, 2019. STEVE, strong thermal emission velocity enhancement.

determined from images at the cadence of our instrument, but appears to indicate the presence of long spatial period wave structures in the STEVE arcs. A highly structured well developed picket fence structure in 557.7-nm was observed after 0502 UT that is, it started 10–12 min after the detachment of the arc from the oval. Green-line emissions from the auroral oval covered the entire northern sky of the ASI during the 0516–0524 UT interval (Movie S2) and the picket fence structure and detached arc disappeared at that time. The picket fence reappeared after 0524 UT but at relatively lower latitude compared to the previous images. While the green arc gave way to widespread aurora in the 0516 to 0524 UT interval (see the 052202 image), the arc in the red-line continued to exist. However, before the green arc reappeared at 0526 UT, the red arc began to fade after ~0520 UT and ceased to exist altogether after 0527 UT (Movie S1). By contrast, the picket fence structure in 557.7 nm intensified again and lasted until 0545 UT.

A notable feature in the 557.7-nm images is the appearance of a black band (highlighted by black arrows in Figure 4b) at the poleward edge of the picket fences, appearing prominently in the interval 0500–0512 UT. This black band is between the equatorward bright green-line arc and diffuse emission of oval aurora poleward of it. Apart from the black band, the sky poleward of the arc in both the red- and green-line images was filled with diffuse faint emission throughout.

In Figure 5, we present NS keograms (in geographic coordinates) to examine the detailed variation of STEVE emissions at different wavelengths. The brightness in the northern sky comes from the auroral oval. The auroral oval expanded until it reached 54.5°N after which it returned poleward after 0500 UT at 630-nm and after 0520 UT in the 557.7-nm emission line. Equatorward of the oval's strong aurora, the presence of a narrow band of emission is discernible in the keogram of all the considered wavelengths, starting after 0455 UT (~2055 MLT). Initially, the arc began to appear at around 54°N in the red-line and at 54.2°N in the other wavelengths. At the time of detachment, the narrow band of emission at 630-nm and 557.7-nm appeared to overlap with the aurora in the oval. At 0506UT, a slight equatorward shift in the red STEVE arc was observed. The red STEVE arc shifted continuously southward from 0512 UT to 0518 UT, displaying a total shift of about 1°. The equatorward motion of STEVE arc is consistent with the findings of earlier researchers (e.g., Gallardo-Lacourt, Liang, 2018; Gallardo-Lacourt, Nishimura, et al., 2018; Liang et al., 2019). At 0518 UT, the arc was found to be located (~53°N) at least 2° latitude equatorward of the auroral oval (~55°N). The emission then became faint after 0518 UT and disappeared entirely after 0524 UT. The faint emission at other wavelengths followed the variation exhibited by 630-nm and also ceased to exist after 0518 UT. By contrast, during the interval 0512–0524 UT, the narrow band structure in the green-line, which came in large part from picket fence emissions, shifted from ~54.2°N to 53.4°N, exhibiting a southward shift of ~1°. The oval aurora overlapped with the detached structures in green-line during ~0512–0525 UT. The arc in 557.7-nm reappeared again after 0525 UT as a faint structure, shifted equatorward, and became brighter at 0530–0536 UT. Afterward, the arc again became faint but existed until ~0545 UT. Picket fence structures in the green-line persisted for about 1 h and were still present after the disappearance of a continuous arc at 630-nm.

3.1.2. Event 2: March 02, 2019

Figure 6 depicts the time sequential airglow images in the red (a) and green (b) line for March 02, 2019. The bright emission in the northern sky of the images for both wavelengths indicates the presence of the auroral oval. A faint latitudinal arc-type structure at the equatorward edge of the auroral oval is observed at 0603

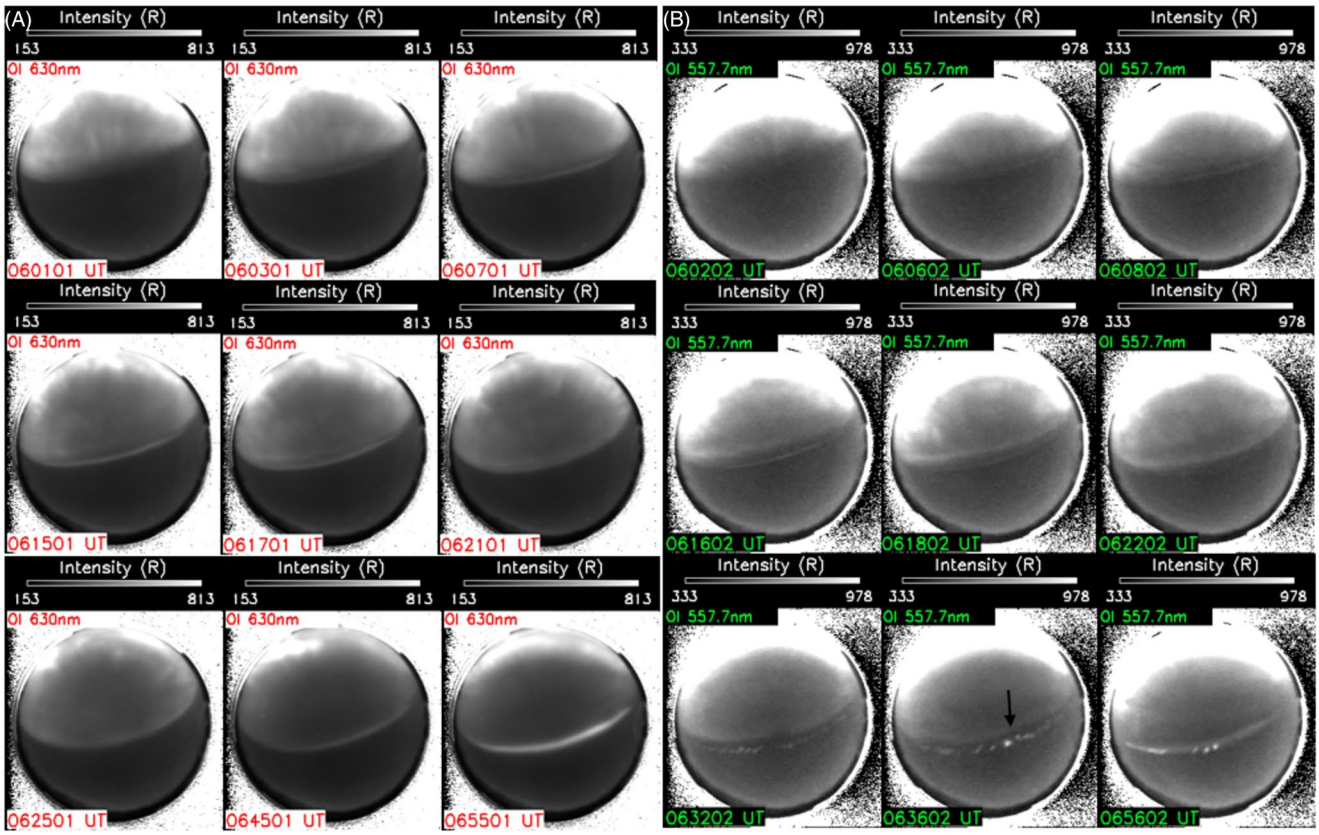

Figure 6. Same as Figure 4 but for March 02, 2019 (during ~0600–0700 UT).

UT in the red-line (Figure 6, Movie S3, and Figure S1). A faint arc-like structure in the green-line (Figure 6, Movie S4, and Figure S1) started to appear at ~0606UT. A faint arc-like structure in OI at 866.6-nm and nonoxygen emission lines (Hbeta, Na, and background; not shown here) is detected at ~0608–0611 UT. A feature noted in the green line is the presence of an additional bright arc at 0616 UT located poleward of the previously existing arc. This new arc, which appeared diffuse as compared to the previously existing arc, moved equatorward, and overlapped with the previously existing arc at 0620 UT. Thereafter, the pre-existing green-line arc faded between 0620 and 0630 UT. The picket fences reached their maximum structuring after 0630 UT and lasted for about one hour, that is, until 0724 UT.

The presence of additional poleward arc-like structure also appeared in the red-line during 0615–0617 UT. This new faint poleward arc in the red-line detached from the auroral oval, moved equatorward, and overlapped with the previously existing structure at 0621 UT. The red-line arc also disappeared for about 10 min that is, at 0635–0643 UT. This arc reappeared from ~0645 UT and became significantly brighter during 0650–0710 UT (see 0655 image). The picket fence structure also was bright during this time. The red-line arc disappeared after 0715 UT and the picket fence structure ceased to exist after 0720 UT. In similarity with the previous case, the sky poleward of the arc in the red-line images was mostly filled by diffuse faint aurora.

Figure 7 depicts the NS keograms at six different wavelengths on March 02, 2019. The bright aurora in the northern sky particularly at 557.7, 630, and 844.6 nm is visible in Figure 7. In the red-line, the auroral oval expanded equatorward until 0600 UT (~55°N) and thereafter returned poleward. The poleward return of the aurora coincided with the detachment of a narrow band of bright emission from the auroral oval. After detachment, the narrow band moved equatorward, brightened at around ~0625 UT, faded out completely at around ~0630 UT, and reappeared as a bright structure at ~0700 UT. This red STEVE arc displayed an equatorward shift of ~1.5° as it appeared at ~53.5°N at 0700 UT and persisted for about 1 h. As in the images, the sky poleward of the arc was filled by faint emissions in this keogram.

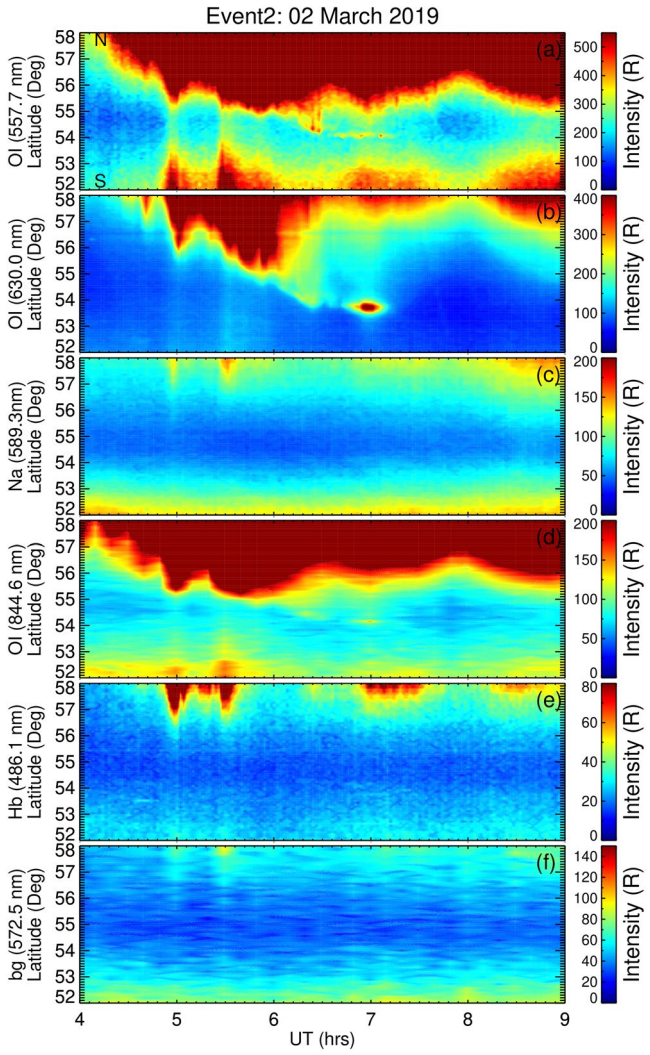

Figure 7. Same as Figure 5 but for March 02, 2019.

In the green-line, a narrow band of bright emission appeared to detach from the auroral oval at 0615 UT. The presence of two bright arcs at ~0615–0630 UT is quite discernible in the green-line keogram. Just like the red-line arc, the arc in the green-line also disappeared at ~0630 UT, and reappeared at 0700 UT as a bright structure. It, too, exhibited a tendency to shift equatorward and shift from 55° to 54°N during the 0610–0700 UT interval. The two bright structures at ~0625 UT and ~0700 UT seen in the red- and green-line are also observed in the 844.6 nm emission line, though at a very weak intensity level. Although the airglow images in Figure 2 at 589.3, 486.1, and 572.5 nm also show the faint arc-like structure during the presence of the arc in the red- and green-line, they do not show with any clarity in the keograms.

3.1.3. Event 3: March 28, 2019

Figure 8a and 8b depicts the sequential images for the red and green lines for March 28, 2019. This event differs from the other two because of the presence of a pre-existing arc in the red line. This pre-existing arc was not accompanied by the picket fence structure in the green-line, nor is it seen in the other wavelengths. At 0823–0825 UT, another faint arc-like feature detached itself from the auroral oval, so that two arcs are visible in the red-line images. This faint arc-like feature brightened later and also shifted equatorward, but remained poleward of the pre-existing arc. In contrast to the previous event, the green-line arc does not show up immediately after the detachment of arc in the red-line. A detectable green-line arc becomes apparent at ~0844 UT (Figures 8b; Movie S6; Figure S2), that is, ~20 min after the detachment of arc in the red-line. The arc in the other emission lines (nonoxygen and OI at 844.6-nm) became detectable from ~0850 UT. The presence of arcs in other emission lines including background emission at ~0850 UT indicates that the initially detached red-line arc at ~0823 UT is indeed a STEVE arc. By comparing the emission intensity of the red-line STEVE arc for all three events, it is observed that the intensity of emission for March 28, 2019 is considerable smaller than the other two events. The pre-existing arc in the red-line became rather faint after 0850 UT perhaps because it was moving eastward away from the ASI field of view. The intensity of the new arc structure in the red-line diminished after 0915 UT (Movie S5) and it ceased to be visible in the ASI field of view after 0925 UT.

In the green-line, a faint arc-like structure started to appear at ~0844 UT (Movie S6). The bright spots in the west side of this detached arc at ~0844 UT could be a weak picket fence. A highly structured well-developed picket fence in the green-line was observed after ~0900 UT and disappeared after ~0930 UT. A weak dark band associated with the picket fence structure (highlighted by black arrow in Figure 8b) was observed at 0902–0906 UT (Movie S6).

In the later phase of the evolution, the arcs in the red (~0847–0910 UT) and green lines (~0900-0910UT) also displayed a ribbon-like motion. This distinct ribbon-like motion of the arcs in both the red and green lines can clearly be identified from Figure 8 and Movies S5 and S6.

Figure 9 depicts NS keograms at six different wavelengths for March 28, 2019. In contrast to the other events, the presence of two arcs was observed in the red-line before the onset of STEVE arc at ~0830 UT. These two arcs detached from the auroral oval, appeared at ~0615–0700 UT and ~0730–0800 UT, and coincided with poleward movement of the auroral oval. Although bright aurora is observed in 481.6, 557.7, and 844.6-nm during the appearance of these arcs, the arc detachment feature is visible only in 630-nm. In the red-line, the auroral oval was located near ~55°N at 0820 UT and showed an equatorward expansion of ~0.5° until ~0830 UT. The detachment of the red-line arc from the auroral oval at ~0830 UT coincided with the poleward movement of the oval. After detachment, the arc moved slightly equatorward and stayed at

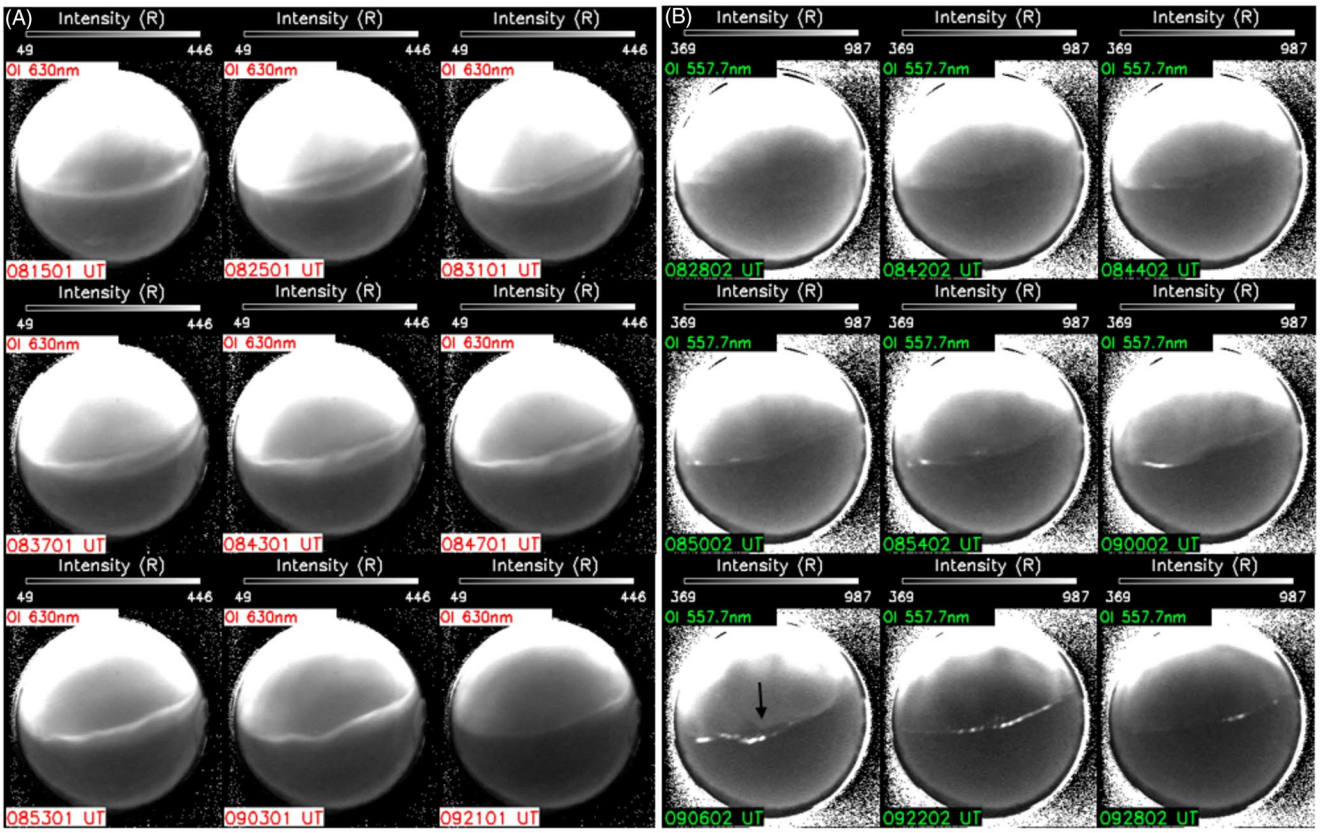

Figure 8. Same as Figure 4 but for March 28, 2019 (during ~0815–0930 UT).

~54°N till 0910 UT. The slight tendency of the poleward movement of the arc at 0910 UT can also be noted. The emission in the red-line show an enhancement at ~0850 UT. The red-line arc persisted for ~40 min and was located about 2° of latitude away from the auroral oval at 0900 UT. In the green-line keogram, the arc-like feature appeared from ~0900 UT at 54.2°N and remains visible for about ~10 min. The faint narrow band of emission is also observed in 844.6-nm at 0830–0900 UT, but it is unclear because of bright light from the poleward aurora. It therefore needed to be highlighted by a black dashed line in Figure 9d. While the faint emission in other wavelengths appeared in the images in Figure 2, they could not be detected in the keograms of 589.3, 486.1, and 572.5 nm.

3.2. Dark Band and Diffuse Emission

For all three events, a notable feature is the appearance of a dark band at the poleward edge of the arc in the green-line and diffuse emissions between the auroral oval and the arcs in the red- and green-line. In this section, we present some detail about the magnitude of the emission intensity of these arcs and their surroundings.

We have plotted the emission intensity as function of latitude by taking the meridional cross-section of the airglow images when the dark band was visible in the green-line emission. The left panels of Figure 10 depict the green-line images for all three STEVE events. The dashed line in the images represents the cross-section location. We have averaged five columns around the meridional cross-section to plot the latitudinal variation of emission intensity, shown in the right panels of Figure 10. The brightness in the northern sky comes from the auroral oval. The prominent peak is the arc in the equatorward side of the auroral oval and it exhibits the picket fence structure. We note the presence of sharp boundaries on both side of the green-arc. The presence of a narrow dark band at the poleward side of the green-line arc is visible in all three STEVE events. These features are clearly discernible in the latitudinal variation of the green-line

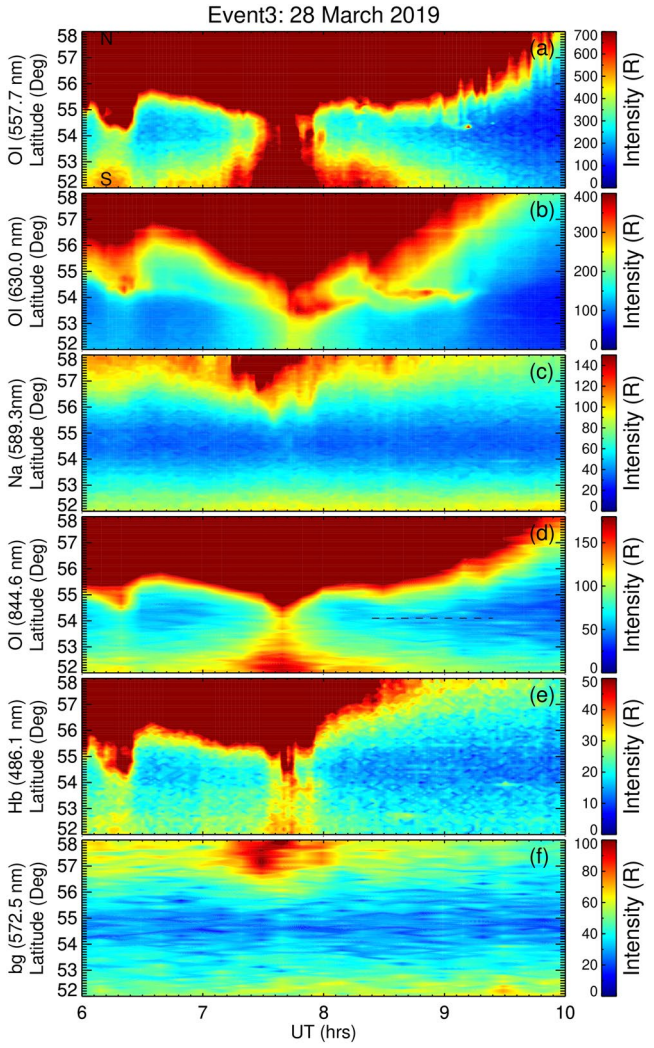

Figure 9. Same as Figure 5 but for March 28, 2019. The dashed black line in Panel (d) highlights the OI emission at 844.6-nm during the presence of arc in the red-line.

emission intensity, shown in the right panels, as the sharp increase in the intensity at ~54°N corresponds to the arc and the narrow negative bay at the immediate poleward side of this arc indicates the presence of a dark band. The latitudinal width of these dark bands is found out to be ~20–30 km. Although the intensity of the emissions decreases steeply as we move away from the oval, the region of lesser emission in the immediate poleward vicinity of the arc is visible as this decrease becomes steeper.

The sky particularly poleward of the arc is filled with diffuse emission. It is clear from the line plots that these diffuse emissions in the green line not only show an abrupt decrease on the poleward side, but also on the equatorward side of the arc. The dark region on the poleward side appears to be more prominent than on the equatorward side. After showing a dip on the equatorward side, the intensity of the green-line displays a gradual increase. The STEVE arc in the green-line is therefore located in the minimum of the diffuse emission region.

In order to examine the magnitude of the emission intensity of the red-line arcs and their surroundings, we have performed a similar analysis for the red-line images and the results are depicted in Figure 11. The emission dip on the poleward side of the arc is also present in the red-line, but with a lesser magnitude as compared to the green-line. The red-line arc appears wider in latitudinal extent than the green-line arc. This may be because of the smearing effect of line-of-sight integration due to wider width of red-line emission at high altitudes and owing to the 110 s delay in the red-line emission. Because of this smaller magnitude of emission dip, the black bands are not visible in the red-line images. Also, by contrast to the green-line, an emission dip is not present on the equatorward side of the arc in the red-lin. Instead, the peak emission intensity of this arc is followed by a steep decrease. Thus, while the green-line arc is located in a broad minimum of emission, the red-line arc appears to be situated at the boundary of the diffuse emissions. The intensity of the green-line arc shows an enhancement by a factor of ~1.5–2 as compared to the poleward negative bay, whereas the red-arc arc shows an increase of about 20%–25% relative to the poleward minimum values.

3.3. Variation of STEVE Emissions With the X-Component of the Magnetic Field at Auroral Latitudes

Broadly speaking, STEVE arcs occur in the recovery phase of the substorm in the three events presented here as well as in previously reported events (Gallardo-Lacourt, Nishimura, et al., 2018). In this subsection, we investigate the effect of additional activities in the recovery phase of the substorm on the STEVE emission. In Figure 12, we have superimposed the X-component of the magnetic field variations observed at FSMI on the NS keograms at 630 and 557.7 nm for our three events. The black solid curve over the keograms depicts the variation of the X-component of the magnetic field at FSMI which is located ~6° magnetic latitude poleward of Athabasca. The magnetic field at FSMI shows abrupt changes in the recovery phase of substorms. As these abrupt changes occurred in the recovery phase of a prevailing substorm, they have been referred to as "additional activity." The correspondence between the movement of the aurora and variations of the ground magnetic field is discernible from Figure 12. The equatorward and poleward movement of equatorward boundary of the auroral oval is associated with the expansion and recovery of the substorm activity observed in terms of decreases and increases in the X-component of the magnetic field at FSMI, respectively. It is observed that STEVE arc detachment, its equatorward movement, and brightness coincided with the presence of additional activity in these magnetic field variations at FSMI.

The quick-look plot of AE/AL index (not shown here) for the event of May 02, 2019 (event 1) showed decreasing/increasing trend during 0240–0600 UT, indicating the presence of a long recovery phase. The

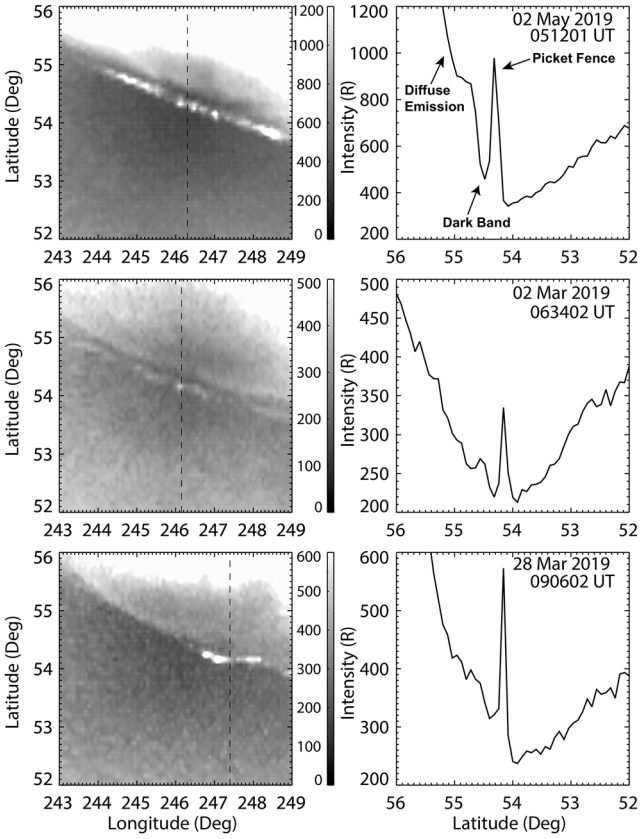

Figure 10. Airglow/auroral images at 557.7-nm for May 02, 2019, March 02, 2019, and March 28, 2019 (left panel). Black dashed lines over the images highlight the meridional cross-section at which the emission intensity is plotted as a function of latitude (right panel).

X-component of the magnetic field showed perturbations between ~0418 and 0442 UT, showing the presence of weaker activity superposed on the overall recovery phase of the substorm (Figure 3). The recovery from the additional activity began after ~0442 UT and the magnetic field X-component showed an enhancement until 0455 UT. This recovery phase coincided with the detachment of a narrow band of emission at ~0450 UT (dashed black line) in both the red and green lines. The X-component of the magnetic field again decreased during the interval ~0455–0505 UT, indicating the presence of further activity in the recovery phase of the substorm. A slight equatorward shift in the arc at 0506 UT in the red-line coincided with the recovery phase of this additional activity marked by the sharp increase in the X-component of the magnetic field, as indicated by dashed black line. Furthermore, the intensification in the green-line arc appeared after the slight increase in the X-component of the magnetic field at ~0527 UT (black dashed line).

For the event of March 02, 2019 (event 2), the decreasing/increasing trend in AE/AL index during ~0530–0730 UT with some additional activity can be identified from the quick-look plots of AE/AL (not shown here). The presence of this additional activity is also observed in the X-component of the magnetic field at FSMI in terms of rapid perturbations during ~0530–0700 UT (Figure 3). The arc detachment in the red- and green-line coincided with the start of the recovery phase of additional activity (dashed black line) and the poleward movement of the auroral oval. The X-component of the magnetic field again showed some additional activity observed in terms of a slight decrease from 0615 UT, reaching a minimum at ~0650 UT, after which it started to increase. This additional activity coincided with the reappearance of the STEVE arc in the red- and green-line, marked by a dashed black line. The STEVE arc in both lines became very bright during the recovery phase of this additional activity.

For the event of March 28, 2019 (event 3), the sharp decrease/increase in the AE/AL index at ~0810–0910 clearly shows the recovery phase of a substorm (quick-look plot of AE/AL, not shown here). In the X-component of the magnetic field at FSMI, the abrupt decrease at ~0810 UT was followed by an increase at 0815 UT. During the recovery phase of this activity, two other sets of perturbations occurred, where the X-component of the magnetic field first decreased and then showed enhancement at 0827 UT and 0858 UT. In response to first additional activity, the aurora oval in the red-line again made an equatorward shift of ~0.5°, and returned poleward from 0830 UT. The STEVE arc detachment in the red-line once again coincided with this additional activity (dashed black line). The second additional activity at ~0858 UT did not cause significant variation in the red-line STEVE aurora, but the brightening of the green-line emission occurred after this change in activity (dashed black line).

4. Discussion

The narrow arcs equatorward of the auroral zone were seen at six wavelengths: 486.1 nm, 572.5 nm, 557.7 nm, 589.3 nm, 630 nm, and 844.6 nm. The 557.7-nm arc evolved into the picket fence structure at the later times. Taken together this indicates that all three events documented in the present work were indeed STEVE events. This paper is providing an unprecedented detailed study of the evolution of STEVE arcs in 630-nm and of lower altitude green-line dominated arcs accompanied by picket fence structures.

This study has uncovered the following interesting features about STEVE: (i) Initially an arc-like faint structure appears very close to the bright auroral oval in the red-line, followed by detectable green and, later on, detectable other emission lines, (ii) the green and red arcs detach themselves from the auroral oval, shifts equatorward, and intensify, (iii) the detachment of the arcs, their equatorward movement, and

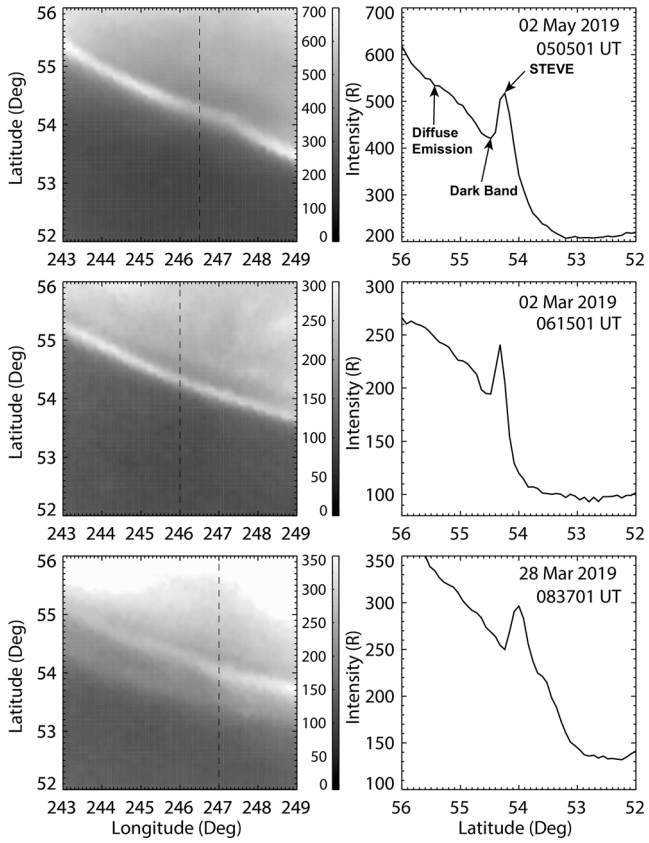

Figure 11. Airglow/auroral images at 630-nm for May 02, 2019, March 02, 2019, and March 28, 2019 (left panel). Black dashed lines over the images highlight the meridional cross-section at which the emission intensity is plotted as a function of latitude (right panel).

their brightness are triggered while there is a sudden change in magnetic activity, as seen in the X-component of the magnetic field. This takes place during the recovery phase of a substorm, (iv) the narrow 630-nm arc evolves into a STEVE as it is associated with emissions in four other wavelengths (i.e., broadband emission), (v) the 557.7-nm arc develops picket fence structures at later times after the arc has moved equatorward, (vi) the picket fence structure in the 557.7-nm emission can sometimes persist after the 630-nm arc itself disappears, (vii) both in 630-nm and 557.7-nm, the arc displays a ribbon-like motion moving through it, (viii) STEVE arc is found to be located in a region of diffuse emissions with sharp boundaries and such boundaries are different for the red- and green-lines, (ix) in all three events, a dark-band is observed in a narrow region 20–30 km wide, poleward of the STEVE arcs, particularly in the green-line.

For the sake of clarity, the discussion has been divided into four subsections. The first subsection deals with the geomagnetic conditions during STEVE. The STEVE arc and picket fence in the green-line are discussed in Section 4.2. The dark band and diffuse emission poleward of the STEVE arc are discussed in Section 4.3 while Section 4.4 describes the multi-wavelength STEVE emissions.

4.1. Substorm Phase and STEVE

Two of three STEVE events were found to occur during positive IMF Bz conditions, suggesting that they may occur under moderately disturbed geomagnetic conditions. Consistent with the study of Gallardo-Lacourt, Nishimura, et al. (2018), STEVE events were found to occur during the recovery phase of substorms. However, a distinctive feature of our results is that arc detachment in the red-line was found to coincide with additional activity in the recovery phase of the substorm. The sudden brightness and equatorward motion of the STEVE arc was also associated with additional activity observed in the X-component of the magnetic field at FSMI. The equatorward motion of the STEVE arc probably corresponds to the inward motion of source plasma in the inner magnetosphere. The present observations suggest that additional activity occurring in the recovery phase of the substorm is an indication of additional energization that might trigger STEVE and cause the increase in brightness.

The initial detachment and equatorward motion of STEVE arc during the substorm recovery phase is similar to the behavior seen in SAR arcs at 630-nm. The poleward movement of the auroral oval immediately after the detachment of a STEVE arc also remains similar to what is found with SAR arcs. Using the Athabasca ASI, Takagi et al. (2018) reported that SAR arcs detached themselves from the high-latitude aurora when the main aurora returned to higher latitudes at the beginning of the substorm recovery phase. This stated, in spite of the similarities in the background conditions under which STEVE and SAR arcs develop, the two phenomena differ markedly from each other. While purple STEVE events are intense enough to be visible to the naked eye, red SAR arcs are weak and remain invisible. SAR arcs are caused by electron heating in the upper F-region at altitudes of ~400 km. The magnetospheric ring current is considered as the ultimate energy source of SAR arcs (e.g., Kozyra et al., 1987). SAR arcs are known to be several hundred kilometers wide in latitude and they may encircle the globe in east-west alignment. By contrast, STEVE is narrow, having a latitudinal width of about half a degree (tens of kilometers) (Gallardo-Lacourt, Nishimura, et al., 2018). STEVE's are associated with the onset of a sharp plasmapause with an intense SAID electric field and thought to involve parallel electron acceleration. These parallel electrons could precipitate and contribute to the STEVE emission in addition to the heat conduction (Chu et al., 2019). The present observations show a correspondence between STEVE and additional magnetic activity in the recovery phase

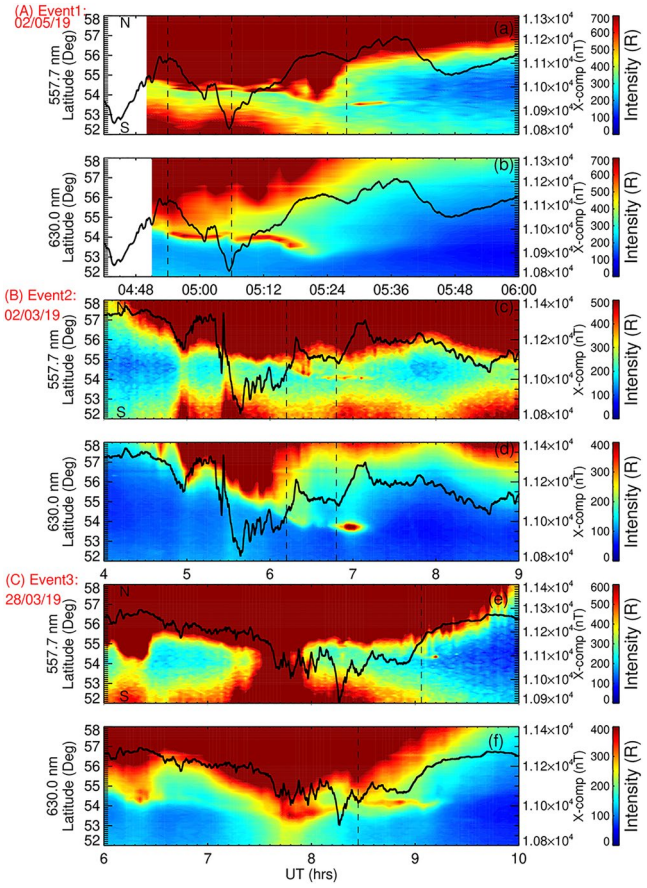

Figure 12. Keograms at red (630-nm) and green (557.7-nm) line for three STEVE events (A) May 02, 2019, (B) March 02, 2019, and (C) March 28, 2019. Black curve superposed on the keograms shows the variation of X-component at Fort Smith (FSMI). Black dashed lines depict the correspondence between evolution of STEVE and the additional activities in the recovery phase of substorm.

of the prevailing substorm, indicating a connection of STEVE with the inner magnetosphere. However, a comprehensive analysis of a statistically significant number of STEVE events is required to substantiate this particular finding.

4.2. STEVE Arc and Picket Fence

At the early phase of detection, the arc in both red- and green-line first appear very close to the auroral oval. As time progresses, this arc detaches itself from the auroral oval and moves equatorward. The detachment and equatorward motion of STEVE has been reported in the earlier studies by using REGO and THEMIS imagers (e.g., Chu et al., 2019; Gallardo-Lacourt, Liang, 2018; Gallardo-Lacourt, Nishimura, et al., 2018; Liang et al., 2019). However, the distinctive aspect of our observations is that in similarity with the arc in the red-line, the green-line arc also appears close to the auroral oval, detaches itself from the auroral oval, and shifts equatorward.

Another notable feature of our multi-wavelength observations is the systematic sequence of arc brightening in different emission lines. A faint narrow arc close to the auroral oval appears first in the red-line followed by green-line and other emission lines. It is interesting to note that green-line arc became intense enough to be detected not long after the red-line arc became visible. The presence of emissions in the nonoxygen emission lines play a decisive role to ascertain the presence of STEVE. The present observations show that there is a time delay when the red-line emission becomes detectable and before other emission lines become detectable. For the event of March 02, 2019, the brightening of arc in other emission lines occurred after a time lag of ~3–5 min, whereas there was a time lag of ~20 min to ascertain the presence of STEVE for the event of March 28, 2019 through the other emissions. Because of the unavailability of images before 0450 UT, we could not examine a possible time lag for the STEVE event of May 02, 2019. The detachable bright arc close to the auroral oval was observed in all the emission lines from the beginning of the observations (0450 UT) for the event of May 02, 2019. The emission intensity of red-line STEVE arc is highest for May 02, 2019 and lowest for March 28, 2019. It is worth mentioning that based on three events, it is not possible to ascertain whether the delay in emissions (between red and other emission lines) is a consequence of brightness or a matter of evolution. Nevertheless, this result raises the question: is the detached arc born as STEVE or does it start as a faint red narrow arc that later evolves into a full-fledged STEVE?

The green-line arc developed picket fence structure after the equatorward movement of the arc rather than at the early phase of their detection. In similarity with the STEVE arc in the 630-nm, the 557.7-nm arc also reveals a ribbon-like motion. These observations suggest that the detached 557.7-nm arc could be the lower altitude part of a unique STEVE. Archer et al. (2019) determined the height range of STEVE (between 130 and 270-km) and picket fence (between 95 and 150-km) through triangulation, suggesting the existence of a lower altitude green STEVE. Liang et al. (2019) by using spectrograph measurements revealed that STEVE was made of two traces, one at a higher elevation angle and the other at a lower elevation angle. The high-altitude STEVE (~250-km) consisted of substantial red-line enhancement over background, while the lower-altitude STEVE (≤150-km) showed enhanced 557.7-nm emission but their magnetic latitude was very similar if not the same They further reported that picket fence displayed collocated airglow continuum structures, indicating a connection between the picket fence and the lower-altitude airglow continuum related to STEVE. However, their result was merely based on a single case study and warranted further investigation. In this context, OMTI monochromatic images have provided new details about the linkage between lower-altitude STEVE, the upper-altitude red STEVE, and the picket fence.

Another distinct feature of present observations is the ribbon-like (wave-like) motion along the STEVE arc. Similar wave-like perturbations have also been observed within SAID in terms of the highly dynamic and localized plasma flows (Foster et al., 2004; Mishin & Burke, 2005; Mishin et al., 2003). Since STEVE is an optical manifestation of SAID, the presence of wavy-motion along the STEVE arc plausibly indicates the presence of long spatial period wave structures, thereby providing a ground-based tool to study long wave perturbations in SAIDs.

4.3. Dark Band and Diffuse Emission

The region between the STEVE arcs and poleward auroral oval is filled with diffuse emissions in both the red and green lines. Associated with this point, a distinctive feature that emerged out of our monochromatic images is that the STEVE arc is located in a region of sharp boundaries. These boundaries are different in red- and green-line. While the green arc is located in a region of broad minimum in the green line diffuse emissions, the red-arc appears at the edge of the diffuse red emissions. The spike of the green-line arc and its boundaries are much sharper compared to the red-line arc. This can be expected on account of a long lifetime (110 s) and altitude spread of the red-line emission. As compared to the poleward minimum, the intensity of the green-line is enhanced by a factor of ∼1.5–2 over the background green emissions, whereas the red-line arc shows a much smaller increase of about 20%–25% over the background red emissions. The sharp decrease in the intensity at the immediate poleward edge of the green-arc is reflected in terms of a "black-band" in the green-line images. These black-bands are reminiscent of east-west aligned arc dark striations reported by G. T. Marklund et al. (1994; 1997) using TV images. The dark striations have been proposed to be "black aurora" in the sense that the emissions are far weaker than in adjacent regions. They have typically been found to be located directly adjacent to auroral arcs (Marklund et al., 1994, 1997). Black auroras have been associated with diverging electric fields and downward field-aligned currents (G. T. Marklund et al., 1994; 1997; 2001 and references therein). While the bright aurora is caused by electrons accelerated toward the earth by an upward pointing field-aligned electric field, it has been proposed that the reverse occurs on adjacent geomagnetic field lines i.e., a downward-pointing field-aligned electric field accelerates electrons away from Earth. Because of the upward flow of ionospheric electrons and the associated evacuation of ions through Pedersen currents lower down, the structures are likely to be associated with localized ionospheric density depletions when compared to the ambient density (e.g., Doe et al., 1993; G. Marklund et al., 1997 and references therein). The resulting localized lack of auroral activity causes the region of diverging electric field to be black (G. T. Marklund et al., 1994; 1997; 2001 and references therein).

4.4. Multi-Wavelength STEVE Emissions

Observations show the presence of hydrogen Balmer lines (Hβ), Na (589.3 nm), 572.5 nm, and 844.6 nm emission in the detached equatorward arc. The emission at 572.5 nm (background emission with no known atomic line origin) supports the notion of the continuum nature of STEVE in the visible part of the spectrum, in agreement with the findings of Gillies et al. (2019). Through the use of a TREx Spectrograph, Gillies et al. (2019) reported an enhanced luminosity of the 630-nm wavelength within STEVE along with an overall enhancement of a continuous spectrum spanning between ∼400 and 730 nm. Liang et al. (2019) also uncovered the presence of STEVE in 486.1 nm (Hβ) and 486 nm (not characteristic of any major auroral/airglow emissions and used for background subtraction), confirming the continuum nature of STEVE.

This conclusion is strengthened by the fact that the background continuum emission monitored at a wavelength of 572.5 nm showed enhancement only within the STEVE structure. It is noted that this emission remained completely absent outside the STEVE structure even in the poleward side of the images where bright aurorae in the oval were observed in the 557.7 nm emission line. The emission at 572.5 nm cannot be interpreted in terms of the band emission from N_2^+ because, in that case, the emission would not be merely restricted within STEVE and would also be visible in the poleward direction where bright aurorae were observed. As a result, we assert that emission feature at 572.5 nm is not caused by the N_2^+ band emission and might be associated with the continuum emission. The sodium lines have been reported to be present at times in the aurora (e.g., Hunten, 1955; Petrie & Small, 1952); however, in the presence case, their strict association with red- and green-line indicates that Na emission is merely a feature of STEVE continuum in the visible range.

Although we believe that OI (844.6 nm) emission could be a part of the continuum, the possibility of its association with particle precipitation cannot be discarded. All three STEVE events presented in this work were associated with a picket fence. Nishimura et al. (2019) reported that the DMSP satellite detects >∼1 keV electron precipitation for STEVE events with picket fence. There might be a possibility that electrons of energies >∼1 keV precipitated from the magnetosphere and caused the OI emissions at 844.6 nm. Chu et al. (2019) also suggested that the superposition of electron precipitation and heat conduction could be behind the multi-wavelength STEVE emissions.

5. Conclusion

We have for the first time examined STEVE arcs in multiple wavelengths which comprise not just the red and green lines of oxygen at 557.7 and 630.0 nm but also emissions at other wavelengths such as Na (589.3 nm), Hβ (486.1 nm), OI (844.6-nm), and bg (572.5 nm). The study is based on three STEVE events which are associated with a picket fence structure at 557.7 nm. The STEVE arc was found to be dominant in the red- and green-line whereas the arc in the other visible wavelengths was very weak. While we could not establish if the green and red arcs shared the same magnetic latitudes owing to their altitude differences, the detailed study on the temporal evolution of the red STEVE arc at 630 nm and the picket fence at 557.7 nm reveals distinct new features about the properties of STEVE. For one thing we could identify the detachment and equatorial motion away from the main auroral oval of STEVE arcs at 630 nm and 557.7 nm separately. The 557.7 nm arc exhibited picket fence structure only at later times, after the arc had moved equatorward. These picket fences could persist even after the 630 nm arc had disappeared. Both in 630 nm and 557.7 nm, the arc displays a ribbon-like motion at times.

Another distinctive feature that emerged from the monochromatic images is that the STEVE arc is embedded in a region of weak diffuse red and green emission. The green emissions from the STEVE sit in a region of broad minimum in the green background emissions, while the red-arc is located at the equatorward edge of the diffuse red emissions. Owing to the very bright emissions in the green STEVE arc, the sharp decrease in the intensity at the immediate poleward edge of the green-arc is reflected in terms of a 'dark-band' in the green-line images having a width of ∼20–30 km.

In order to investigate the association of STEVE with magnetospheric activity, we have examined the variation of magnetic field X-component at FSMI during the evolution of STEVE arcs. At the times of interest FSMI was located in the auroral oval at the longitude of Athabasca. Results show that the detachment of STEVE arcs from the auroral oval, their equatorward movement, and sudden brightening coincided with additional activity, namely, changes in the X-component of the magnetic field, during substorm recovery phases.

Data Availability Statement

The optical data obtained at Athabasca are available through ISEE/Nagoya University. Quick-look plots of the OMTI data are available at http://stdb2.isee.nagoya-u.ac.jp/omti/and the data can be accessed from the ERG Science Center operated by ISAS/JAXA and ISEE/Nagoya University (https://ergsc.isee.nagoya-u.ac.jp/data/ergsc/ground/camera/omti/asi/). The solar wind parameters and X-component data at Fort Smith were obtained from SPDF, NASA, USA (https://cdaweb.gsfc.nasa.gov/index.html/). The FSMI data used in this study is a part of Canadian Array for Realtime Investigations of Magnetic Activity (CARISMA) (Mann et al., 2008).

Acknowledgment
JPSTM acknowledges ISEE, Nagoya University, Japan for hosting him as a visiting designated professor for two months. The all-sky imager at Gakona was calibrated using optical facilities of National Institute of Polar Research, Japan (Ogawa et al., 2020). This work is supported by JSPS KAKENHI (15H05815 and 16H06286). The Athabasca University GeoSpace Observatory was built and is operated with support from the Canada Foundation for Innovation. M.C. and JPSM both acknowledge support from Canada's NSERC.

References

Archer, W. E., Gallardo-Lacourt, B., Perry, G. W., St-Maurice, J.-P., Buchert, S. C., & Donovan, E. F. (2019). Steve: The optical signature of intense subauroral ion drifts. *Geophysical Research Letters*, *46*, 6279–6286. https://doi.org/10.1029/2019GL082687

Archer, W. E., St-Maurice, J.-P., Gallardo-Lacourt, B., Perry, G. W., Cully, C. M., Donovan, E., et al. (2019). The vertical distribution of the optical emissions of a Steve and Picket Fence event. *Geophysical Research Letters*, *46*, 10719–10725. https://doi.org/10.1029/2019GL084473

Chu, X., Malaspina, D., Gallardo-Lacourt, B., Liang, J., Andersson, L., Ma, Q., et al. (2019). Identifying STEVE's magnetospheric driver using conjugate observations in the magnetosphere and on the ground. *Geophysical Research Letters*, *46*, 12665–12674. https://doi.org/10.1029/2019GL082789

Doe, R. A., Mendillo, M., Vickrey, J., Zanetti, L., & Eastes, R. (1993). Observations of nightside auroral cavities. *Journal of Geophysical Research*, *98*, 293–310.

Foster, J. C., Erickson, P. J., Lind, F. D., & Rideout, W. (2004). Millstone Hill coherent-scatter radar observations of electric field variability in the sub-auroral polarization stream. *Geophysical Research Letters*, *31*, L21803. https://doi.org/10.1029/2004GL021271

Gallardo-Lacourt, B., Liang, J., Nishimura, Y., & Donovan, E. (2018). On the origin of STEVE: Particle precipitation or ionospheric skyglow?. *Geophysical Research Letters*, *45*, 7968–7973. https://doi.org/10.1029/2018GL078509

Gallardo-Lacourt, B., Nishimura, Y., Donovan, E., Gillies, D. M., Perry, G. W., Archer, W. E., et al. (2018). A statistical analysis of STEVE. *Journal of Geophysical Research: Space Physics*, *123*, 9893–9905. https://doi.org/10.1029/2018JA025368

Gillies, D. M., Donovan, E., Hampton, D., Liang, J., Connors, M., Nishimura, Y., et al. (2019). First observations from the TREx Spectrograph: The optical spectrum of STEVE and the Picket Fence phenomena. *Geophysical Research Letters*, *46*, 7207–7213. https://doi.org/10.1029/2019GL083272

Hunten, D. M. (1955). Some photometric observations of auroral spectra. *Journal of Atmospheric and Terrestrial Physics*, *7*, 141–151. https://doi.org/10.1016/0021-9169(55)90121-5

Kozyra, J. U., Shelley, E. G., Comfort, R. H., Brace, L. H., Cravens, T. E., & Nagy, A. F. (1987). The role of ring current O+ in the formation of stable auroral red arcs. *Journal of Geophysical Research*, *92*(A7), 7487–7502. https://doi.org/10.1029/JA092iA07p07487

Liang, J., Donovan, E., Connors, M., Gillies, D., St-Maurice, J. P., Jackel, B., et al. (2019). Optical spectra and emission altitudes of double-layer STEVE: A case study. *Geophysical Research Letters*, *46*, 13630–13639. https://doi.org/10.1029/2019GL085639

MacDonald, E. A., Donovan, E., Nishimura, Y., Case, N. A., Gillies, D. M., Gallardo-lacourt, B., et al. (2018). New science in plain sight: Citizen scientists lead to the discovery of optical structure in the upper atmosphere. *Science Advances*, *4*, 16–21. https://doi.org/10.1126/sciadv.aaq0030

Mann, I. R., et al. (2008). The upgraded CARISMA magnetometer array in the THEMIS era. *Space Science Reviews*, *141*, 413–451. https://doi.org/10.1007/s11214-008-9457-6

Marklund, G. T., et al. (2001). Temporal evolution of the electric field accelerating electrons way from the auroral ionosphere. *Nature*, *414*, 724. https://doi.org/10.1038/414724a

Marklund, G. T., Blomberg, L. G., Fälthammar, C.-G., & Lindqvist, P.-A. (1994). On intense shock-like electric fields associated with black aurora. *Geophysical Research Letters*, *21*, 1859–1862.

Marklund, G., Karlsson, T., & Clemmons, J. (1997). On low-altitude particle acceleration and intense electric fields and their relationship to black aurora. *Journal of Geophysical Research*, *102*, 17509–17522.

Mende, S. B., Harding, B. J., & Turner, C. (2019). Subauroral green STEVE arcs: Evidence for low-energy excitation. *Geophysical Research Letters*, *46*, 14256–14262. https://doi.org/10.1029/2019GL086145

Mishin, E. V., & Burke, W. J. (2005). Stormtime coupling of the ring current, plasmasphere, and topside ionosphere: Electromagnetic and plasma disturbances. *Journal of Geophysical Research*, *110*, A07209. https://doi.org/10.1029/2005JA011021

Mishin, E. V., Burke, W. J., Huang, C. Y., & Rich, F. J. (2003). Electromagnetic wave structures within subauroral polarization streams. *Journal of Geophysical Research*, *108*(A8), 1309. https://doi.org/10.1029/2002JA009793

Nishimura, Y., Gallardo-Lacourt, B., Zou, Y., Mishin, E. V., & Knudsen, D. J. (2019). Magnetospheric signatures of STEVE: Implication for the magnetospheric energy source and inter-hemispheric conjugacy. *Geophysical Research Letters*, *46*, 5637–5644. https://doi.org/10.1029/2019GL082460

Ogawa, Y., Kadokura, A., & Ejiri, M. K. (2020). Optical calibration system of NIPR for aurora and airglow observations. *Polar Science*, *26*, 100570. https://doi.org/10.1016/j.polar.2020.100570

Petrie, W., & Small, R. (1952). Auroral spectrum in the wavelength range 3300–8900Å. *The Astrophysical Journal*, *116*, 433–441.

Shiokawa, K., Katoh, Y., Satoh, M., Ejiri, M. K., Ogawa, T., Nakamura, T., et al. (1999). Development of optical mesosphere thermosphere imagers (OMTI). *Earth Planets and Space*, *51*, 887–896.

Shiokawa, K., Otsuka, Y., & Ogawa, T. (2009). Propagation characteristics of nighttime mesospheric and thermospheric waves observed by optical mesosphere thermosphere imagers at middle and low latitudes. *Earth Planets and Space*, *61*, 479–491.

Takagi, Y., Shiokawa, K., Otsuka, Y., Connors, M., & Schofield, I. (2018). Statistical analysis of SAR arc detachment from the main oval based on 11-year, all-sky imaging observation at Athabasca, Canada. *Geophysical Research Letters*, *45*, 11539–11546. https://doi.org/10.1029/2018GL079615